Article

Zinc-Amyloid β Interactions on a Millisecond Time-Scale Stabilize Non-fibrillar Alzheimer-Related Species

Dror Noy, Inna Solomonov, Ory Sinkevich, Talmon Arad, Kristian Kjaer, and Irit Sagi

J. Am. Chem. Soc., **2008**, 130 (4), 1376-1383 • DOI: 10.1021/ja076282l

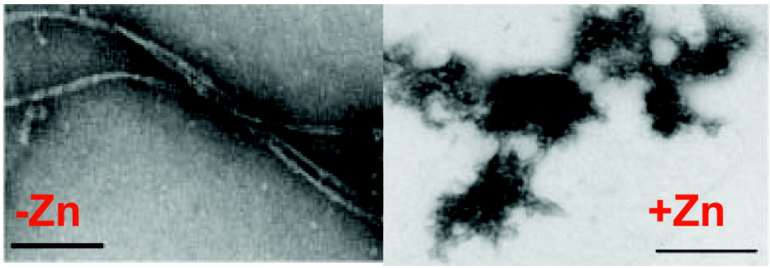

J|A|C|S
ARTICLES
Published on Web 01/08/2008

Zinc-Amyloid β Interactions on a Millisecond Time-Scale Stabilize Non-fibrillar Alzheimer-Related Species

Dror Noy,[†] Inna Solomonov,[†] Ory Sinkevich,[†] Talmon Arad,[‡] Kristian Kjaer,[§] and Irit Sagi*,[†]

Structural Biology Department and Electron Microscopy Unit, Weizmann Institute of Science, Rehovot 76100, Israel, and Niels Bohr Institute, University of Copenhagen, Universitesparken 5, DK-2100, Copenhagen, Denmark

Received August 31, 2007; E-mail: irit.sagi@weizmann.ac.il

Abstract: The role of zinc, an essential element for normal brain function, in the pathology of Alzheimer's disease (AD) is poorly understood. On one hand, physiological and genetic evidence from transgenic mouse models supports its pathogenic role in promoting the deposition of the amyloid β-protein (Aβ) in senile plaques. On the other hand, levels of extracellular ("free") zinc in the brain, as inferred by the levels of zinc in cerebrospinal fluid, were found to be too low for inducing Aβ aggregation. Remarkably, the release of transient high local concentrations of zinc during rapid synaptic events was reported. The role of such free zinc pulses in promoting Aβ aggregation has never been established. Using a range of time-resolved structural and spectroscopic techniques, we found that zinc, when introduced in millisecond pulses of micromolar concentrations, immediately interacts with Aβ 1−40 and promotes its aggregation. These interactions specifically stabilize non-fibrillar pathogenic related aggregate forms and prevent the formation of Aβ fibrils (more benign species) presumably by interfering with the self-assembly process of Aβ. These in vitro results strongly suggest a significant role for zinc pulses in Aβ pathology. We further propose that by interfering with Aβ self-assembly, which leads to insoluble, non-pathological fibrillar forms, zinc stabilizes transient, harmful amyloid forms. This report argues that zinc represents a class of molecular pathogens that effectively perturb the self-assembly of benign Aβ fibrils, and stabilize harmful non-fibrillar forms.

Introduction

Despite compelling physiological and genetic evidence,[1−6] the actual role of zinc (Zn) in the pathology of Alzheimer's disease (AD) is unclear. The underlying assumption attributes the toxic effects of Zn (an essential element for normal neural function)[7,8] to its interactions with the amyloid-β peptide (Aβ).[7,9−11] This induces Aβ misfolding and aggregation that leads to neural cell damage either directly, or by triggering the inflammatory glial response.[7,12,13] However, as inferred from levels of Zn in cerebrospinal fluid, the extracellular levels of exchangeable Zn ions in normal healthy brain, on the order of 1−10 nM, are too low for significant complex formation with Aβ, which requires about 10 to 100-fold higher concentration for significant Zn binding and more than 1000-fold higher concentration to trigger Aβ misfolding and aggregation in vitro.[14,15] Nevertheless, recent studies of transgenic mouse models of AD demonstrated significant reduction in loads of cerebral senile plaques (SP), the pathological hallmark of AD,[16,17] either by knocking out the gene for the synaptic vesicle transporter ZnT3[3] or by treatment with the metal chelator drug clioquinol.[1,2]

Frederickson et al. have shown that some neurons store up to 200−600 μM of Zn, and are able to release about 1−10% of

[†] Structural Biology Department, Weizmann Institute of Science.
[‡] Electron Microscopy Unit, Weizmann Institute of Science.
[§] Niels Bohr Institute, University of Copenhagen.

(1) Cherny, R. A.; Atwood, C. S.; Xilinas, M. E.; Gray, D. N.; Jones, W. D.; McLean, C. A.; Barnham, K. J.; Volitakis, I; Fraser, F. W.; Kim, Y. S.; Huang, X.; Goldstein, L. E.; Moir, R. D.; Lim, J. T.; Beyreuther, K.; Zheng, H. T. *Neuron* **2001**, *30*, 665−676.
(2) Opazo, C.; Luza, S.; Villemagne, V. L.; Volitakis, I.; Rowe, C.; Barnham, K. J.; Strozyk, D.; Masters, C. L.; Cherny, R. A.; Bush, A. I. *Aging Cell* **2006**, *5*, 69−79.
(3) Lee, J. Y.; Cole, T. B.; Palmiter, R. D.; Suh, S. W.; Koh, J. Y. *Proc. Natl. Acad. Sci. U.S.A.* **2002**, *99*, 7705−7710.
(4) Dong, J.; Atwood, C. S.; Anderson, V. E.; Siedlak, S. L.; Smith, M. A.; Perry, G.; Carey, P. R. *Biochemistry* **2003**, *42*, 2768−2773.
(5) Miller, L. M.; Wang, Q.; Telivala, T. P.; Smith, R. J.; Lanzirotti, A.; Miklossy, J. *J. Struct. Biol.* **2006**, *155*, 30−37.
(6) Religa, D.; Strozyk, D.; Cherny, R. A.; Volitakis, I.; Haroutunian, V.; Winblad, B.; Naslund, J.; Bush, A. I. *Neurology* **2006**, *67*, 69−75.
(7) Bush, A. I. *Trends Neurosci.* **2003**, *26*, 207−214.
(8) Maynard, C. J.; Bush, A. I.; Masters, C. L.; Cappai, R.; Li, Q. X. *Int. J. Exp. Pathol.* **2005**, *86*, 147−159.
(9) Ali, F. E. A.; Barnham, K. J.; Barrow, C. J.; Separovic, F. *Aust. J. Chem.* **2004**, *57*, 511−518.
(10) Lacor, P. N.; Buniel, M. C.; Furlow, P. W.; Clemente, A. S.; Velasco, P. T.; Wood, M.; Viola, K. L.; Klein, W. L. *J. Neurosci.* **2007**, *27*, 796−807.
(11) Townsend, M.; Shankar, G. M.; Mehta, T.; Walsh, D. M.; Selkoe, D. J. *J. Physiol. (Lond.)* **2006**, *572*, 477−492.
(12) Huang, X. D.; Atwood, C. S.; Hartshorn, M. A.; Multhaup, G.; Goldstein, L. E.; Scarpa, R. C.; Cuajungco, M. P.; Gray, D. N.; Lim, J.; Moir, R. D.; Tanzi, R. E.; Bush, A. I. *Biochemistry* **1999**, *38*, 7609−7616.
(13) Huang, X. D.; Cuajungco, M. P.; Atwood, C. S.; Hartshorn, M. A.; Tyndall, J. D. A.; Hanson, G. R.; Stokes, K. C.; Leopold, M.; Multhaup, G.; Goldstein, L. E.; Scarpa, R. C.; Saunders, A. J.; Lim, J.; Moir, R. D.; Glabe, C.; Bowden, E. F.; Masters, C. L.; Fairlie, D. P.; Tanzi, R. E.; Bush, A. I. *J. Biol. Chem.* **1999**, *274*, 37111−37116.
(14) Bush, A. I.; Pettingell, W. H.; Multhaup, G.; Paradis, M. D.; Vonsattel, J. P.; Gusella, J. F.; Beyreuther, K.; Masters, C. L.; Tanzi, R. E. *Science* **1994**, *265* (5177), 1464−1467.
(15) Bush, A. I.; Pettingell, W. H.; Paradis, M. D.; Tanzi, R. E. *J. Biol. Chem.* **1994**, *269*, 12152−12158.
(16) Kidd, M. *Nature* **1963**, *197*, 192−193.
(17) Terry, R. D. *J. Neuropathol. Exp. Neurol.* **1963**, *22*, 629−642.

10.1021/ja076282l CCC: $40.75

this amount from their presynaptic terminals as "pulses" of freely exchangeable Zn ions.[18] The spatial and temporal profiles of these synaptic pulses were characterized by fluorescence imaging techniques showing a temporary rise of Zn ion concentrations of 10−30 μM within ∼30 ms and a decay with a half-life of several seconds.[19] Interactions of Zn with Aβ in this time domain have not yet been studied.

Here, we present in vitro experimental evidence that links rapid physiological Zn release with the formation of possibly pathogenically related Zn-containing aggregate forms of Aβ. By combining molecular and structural dynamic studies from various time-resolved spectroscopic experiments with molecular to microscopic scales, we were able to gain critical dynamic insights about the molecular events involved in Aβ aggregation and fibrillation. We show, for the first time, that the early interactions between Zn and Aβ occur within milliseconds under typical synaptic Zn release concentrations. Most importantly, we confirm that micromolar Zn concentrations significantly stabilize non-fibrillar forms of Aβ 1−40 and prevent the formation of amyloid fibrils. This may imply a specific role for Zn in promoting Aβ pathology in AD as recent reports demonstrate that these forms are much more potent neurotoxins than the mature amyloid fibrils.[10,11,20] Structural characterization of early aggregate species reveals multiple metal binding sites that have minimal effect on the overall core molecular structure of Aβ 1−40.

Materials and Methods

Aβ 1−40 Synthesis and Sample Preparation. Buffer and Zn solutions were prepared with deionized water from a Milli-Q water purification system (Millipore, USA), and analytical grade reagents. Aβ 1−40 was synthesized and purified at the protein synthesis core facility of the Weizmann Institute of Science by standard solid-phase synthesis using FMOC chemistry, and reversed-phase HPLC, respectively. The peptide purity and integrity was verified by electrospray mass spectrometry (ES−MS). All peptide samples yielded the expected molecular weight of 4328 D and were >97% pure. Aβ 1−40 stock solutions were prepared by dissolving in 10 mM NaOH (Sigma−Aldrich, Israel) to concentrations of 200−800 μM and sonicating for 1 min in a bath sonicator. Analytical ultracentrifugation (AUC) measurements (not shown) have verified that under these conditions, the stock solutions are purely monomeric. These solutions could be kept for several days at 4 °C and were resonicated prior to use. Buffered samples were prepared by diluting stock solutions with 150 mM MOPS (Sigma-Aldrich, Israel) solution at pH 6.9.

Kinetic Studies. Kinetic measurements were performed in a stopped-flow apparatus (SFM-300, Bio-Logic, Claix, France) equipped with a photomultiplier tube masked by a 290 nm high-wavelength pass optical filter (CVI, Albuquerque NM). The total fluorescence intensity of the single native tyrosine residue of Aβ 1−40, and the Rayleigh light scattering intensity were monitored by setting the excitation wavelength to 276 and 435 nm, respectively. Reactions were initiated by mixing a buffered Aβ 1−40 solution with pure buffer solution, and $ZnCl_2$ (Sigma-Aldrich, Israel) solution into a fluorescence cuvette with an optical path length of 0.8 mm. The total mixing volume in the cuvette was 15.6 μL, and the mixing flow rate was 3.2 mL/s; hence, the dead-time of the instrument was approximately 5 ms. A special mixing sequence was designed in order to allow proper normalization of signal intensities from Zn/Aβ 1−40 mixtures with respect to Zn-free Aβ 1−40 (for a detailed description, see Supporting Information).

Transmission Electron Microscopy (TEM). Freshly prepared 50 μM Aβ 1−40 in MOPS was split into two aliquots, and a concentrated stock of $ZnCl_2$ was immediately added to one of them at a final concentration of 100 μM. The solutions were aged at 25 °C without agitation and were sampled at given time points from t_0, corresponding to ∼2 min to over 10 days. Five-microliter aliquots from each solution were diluted 2-fold with buffer, deposited on carbon coated grids, and stained with 1% w:v aqueous uranyl acetate. These samples were observed in a Tecnai 12 Transmission Electron Microscope (FEI, Eindhoven, The Netherlands), operated at 120kV. Micrographs were taken with MegaView III CCD camera (SIS, Muenster, Germany).

Sedimentation Velocity. Sedimentation velocity measurements were performed in a Beckman XLA analytical ultracentrifuge equipped with an eight-hole rotor. Samples (0.4 mL) of 50 μM Aβ 1−40 were freshly prepared with 0, 5, 25, and 50 μM Zn, loaded into standard two-channel cells, placed in the rotor and left to equilibrate at rest in the centrifuge. To reduce equilibration time, the run temperature was set as close as possible to the rotor temperature typically 20−22 °C, and the run started 2 h after reaching this temperature.

Measurements were run at 50 000 rpm for 15−18 h. Zn-free samples were kept in their cells after the first measurement, agitated vigorously to eliminate any concentration gradients, and kept at 37 °C for 3 days, after which a second measurement was performed. Sedimentation coefficient distributions, $c(s)$, were obtained from the raw data by using the software Sedfit[21] (obtained from http:// www.analyticalultracentrifugation.com).

Grazing Angle X-ray Diffraction (GIXD). A detailed description of GIXD applied to films on liquid surfaces has been given elsewhere.[22,23] Here, experiments were performed on the liquid surface diffractometer at the BW1 undulator beam line at the HASYLAB synchrotron source at Deutsches Elektronen−Synchrotron, Hamburg, Germany. Aβ 1−40 films were produced by injecting a stock solution into the buffered bulk in a Langmuir trough adjusting the final peptide concentration to ∼500 nM. Then, the trough was tightly closed and flushed with helium to reduce X-ray background scattering. The X-ray diffraction measurements were performed at 22 °C. To maximize surface sensitivity, a monochromatic X-ray beam was adjusted to strike the liquid surface at an incident angle $\alpha_i < 0.85\alpha_c$, where α_c is the critical angle for total external reflection.

Time-Resolved X-ray Absorption Spectroscopy. Samples were prepared using a freeze−quench apparatus as previously described.[24] XAS data collection was performed at beam-line 7.1 of Daresbury Synchrotron Radiation Source (SRS) at Daresbury, UK. Spectra were recorded at the Zn K-edge in fluorescence geometry at low temperature (30 °K) to reduce thermal disorder. The beam energy was defined using a flat Si (111) monochromator crystal. The incident beam intensity, I_0, was recorded using an ionization chamber. The fluorescence intensity was recorded using a 13-element germanium detector. Several scans of each sample were collected for a total of 10^6 counts across the edge or until a good statistic was obtained. Samples were checked for burning marks after each scan, and the beam position on the sample was changed before each scan to minimize radiation damage.

Data Analysis and Modeling. General data analysis, global fitting, and principal component analysis were carried out with the software Igor Pro 5.0 (Wavemetrics, Lake-Oswego OR). The iterative key sets factor analysis algorithm[25] was implemented in "Igor Pro" using the software's scripting language. Coordinates for the molecular models of Aβ 1−40 fibrils[26] were kindly provided by Dr. Robert Tycko,

(18) Frederickson, C. J.; Koh, J. Y.; Bush, A. I. *Neurosci.* **2005**, *6*, 449−462.
(19) Li, Y.; Hough, C. J.; Suh, S. W.; Sarvey, J. M.; Frederickson, C. J. *J. Neurophysiol.* **2001**, *86*, 2597−2604.
(20) Caughey, B.; Lansbury, P. T. *Annu. Rev. Neurosci.* **2003**, *26*, 267−298.
(21) Schuck, P. *Biophys. J.* **2000**, *78*, 1606−1619.
(22) Als-Nielsen, J.; Jacquemain, D.; Kjaer, K.; Leveiller, F.; Lahav, M.; Leiserowitz, L. *Phys. Rep.* **1994**, *246*, 252−313.
(23) Kuzmenko, I.; Rapaport, H.; Kjaer, K.; Als-Nielsen, J.; Weissbuch, I.; Lahav, M.; Leiserowitz, L. *Chem. Rev.* **2001**, *101*, 1659−1696.
(24) Kleifeld, O.; Frenkel, A.; Martin, J. M. L.; Sagi, I. *Nat. Struct. Biol.* **2003**, *10*, 98−103.
(25) Malinowski, E. R. *Factor Analysis in Chemistry*, 3rd ed.; John Wiley: New York, 2002.
(26) Petkova, A. T.; Yau, W. M.; Tycko, R. *Biochemistry* **2006**, *45*, 498−512.

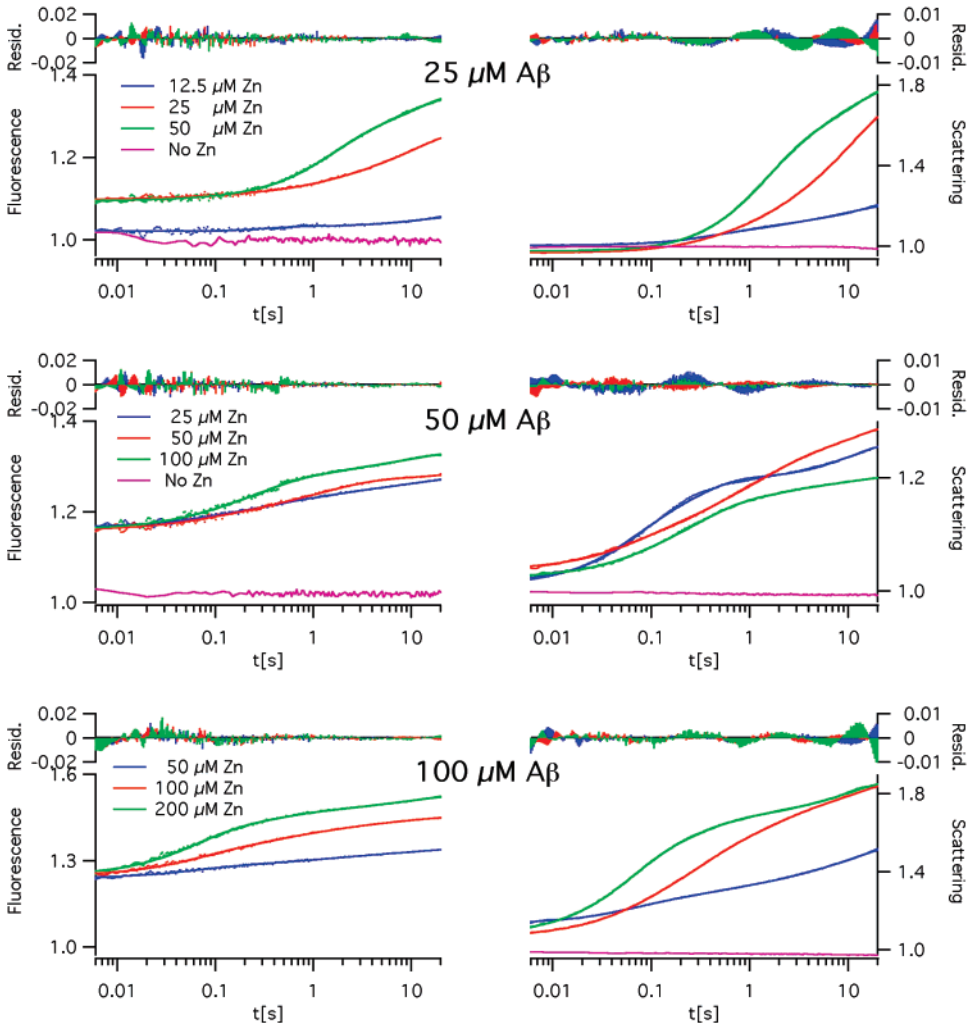

Figure 1. Normalized scattering (right) and tyrosine fluorescence (left) traces of 25 μM (top) 50 μM (middle) and 100 μM (bottom) Aβ 1−40 rapidly mixed with Zn to molar ratios of 1:2, 1:1, and 2:1 Zn:Aβ compared to control samples without Zn. Recorded signals (dots) were fitted with four-exponential decay curves (solid lines) and the residuals plots for each fit are shown on top of each graph.

Laboratory of Chemical Physics, NIDDK, National Institute of Health, Bethesda MD. These were slightly manipulated by changing the relative positions of individual monomers in order to form the conformations presented in Figure 6. Additionally, two α-helical conformations of Aβ 1−40 monomers (Figure 6, top) were obtained from a structure posted in the protein data bank (PDB Code: 1BA4). Visualization and coordinates manipulation were performed with the program VMD.[27]

Results

Aβ Aggregation is Induced by Zn in Milliseconds. The local and rapid discharge of extracellular Zn from Zn-releasing neurons during normal brain function has prompted us to study the kinetics of Zn binding and the misfolding of Aβ on a similar time-scale. Therefore, we used rapid mixing techniques in a stopped-flow apparatus to monitor the fluorescence intensity of the single native tyrosine residue of Aβ 1−40, Y10, and the Rayleigh light scattering intensity as direct internal probes of changes in Aβ 1−40 conformation and aggregation states, respectively, with time resolution on the order of milliseconds.

Figure 1 shows rapid and dramatic changes in normalized Y10 fluorescence and Rayleigh scattering intensity detected upon mixing the Aβ 1−40 peptide with stoichiometric $ZnCl_2$ solutions whereas, in contrast, the fluorescence of control samples comprising Aβ 1−40 mixed with the same buffer solution without metals remained essentially constant over the same time range. The final Zn concentrations, ranging from 25 to 100 μM, and the rapid sample mixing time of ∼5 ms represent typical synaptic Zn release conditions. In this setting, the kinetics of both fluorescence and scattering signals clearly indicate significant Aβ 1−40 conformational and aggregate size changes during the first milliseconds to seconds. This multiexponential kinetics depends on peptide and Zn concentrations. This complicated the assignment of any specific kinetic mechanism. Moreover, the initial fluorescence signals, which reflect changes in the local environment of Y10 are significantly offset with respect to the signal without metals, whereas the initial scattering intensity, which is sensitive to aggregate size distribution, is usually closer to baseline levels (Figure 1B). This indicates that early conformational changes occur faster than the instrument's response time of ∼5 ms. Furthermore, since fluorescence specifically probes the direct electronic environment of Y10 whereas scattering is sensitive to the protein aggregation number, it is likely that early intermediates involve either direct Zn-Y10 interactions, and/or conformational changes affecting its immediate environment. Later, these changes trigger fast Aβ

(27) Humphrey, W.; Dalke, A.; Schulten, K. *J. Mol. Graphics* **1996**, *14*, 33−38.

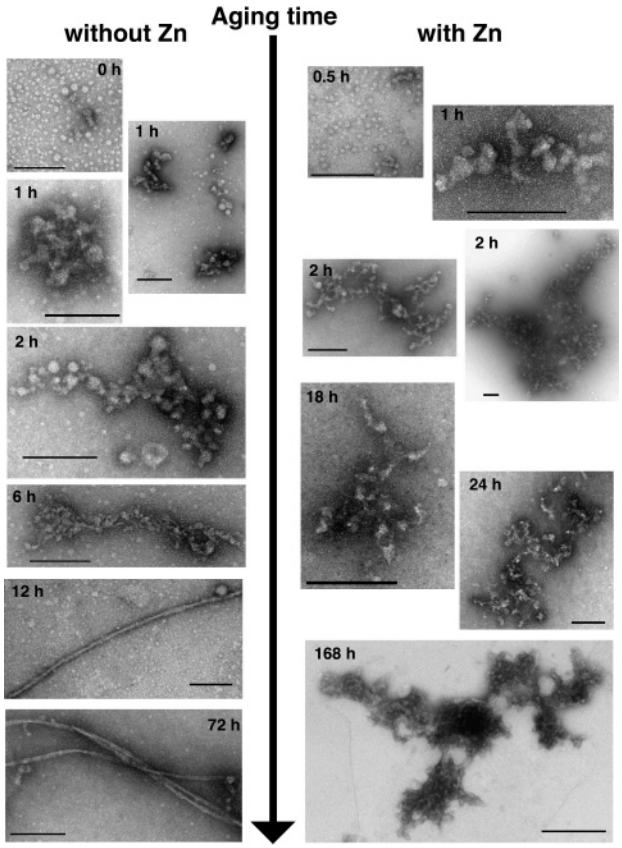

Figure 2. Evolution of Aβ 1−40 aggregate morphology with and without Zn. TEM images of Aβ 1−40 samples with and without Zn were recorded at various aging times from $t = 0$ h (equivalent to ∼2 min after sample preparation) up to $t = 168$ h (one week). The typical elongated fibrils observed in Zn-free sample (12 and 72 h images) were not detected at any time in Zn-containing samples.

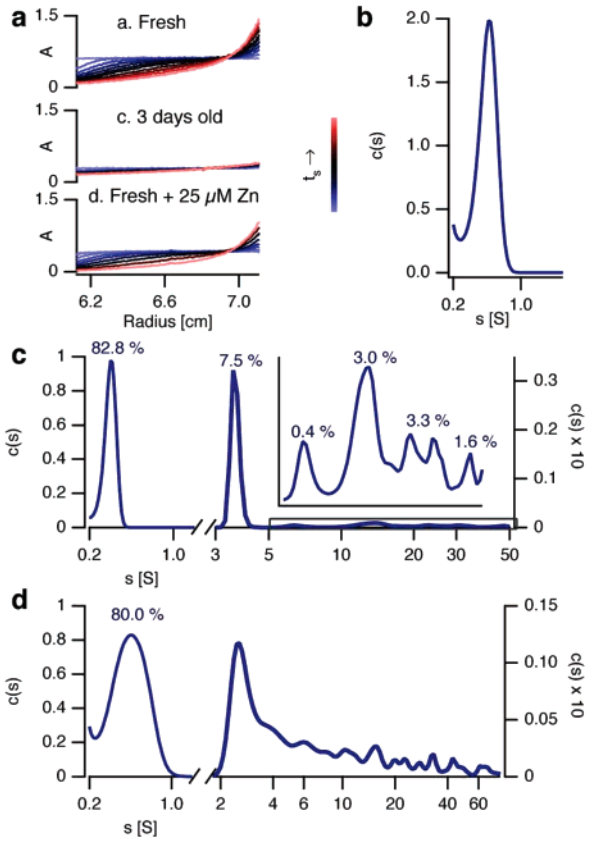

Figure 3. Sedimentation velocity profiles of freshly prepared 50 μM Aβ 1−40 (a. top) indicate primarily monomeric species but when the same sample was measured after incubation for 3 days at 37 °C (a. middle), or when 25 μM Zn is added to the fresh sample (a. bottom), very high-molecular weight aggregates (more than 10^5 kD) are formed and sediment during the acceleration phase of the centrifuge as reflected by the significant loss of total absorption signals compared to the fresh sample. The sedimentation coefficient distribution, $c(s)$, plots reveal a homogeneous solution of low-molecular weight species in the freshly prepared Zn-free sample (b). Yet, despite the significant sedimentation, $c(s)$ plots of 3 days old Zn-free, and fresh Zn-containing samples (c, and d, respectively) indicate that only ∼20% of the remaining Aβ 1−40 species in solution are aggregates and the rest are low molecular-weight species. The aggregate size distribution of fresh Zn-containing sample is broad, continuous, and includes larger aggregates, whereas the aged Zn-free sample contains aggregates of only a few distinct sizes.

1−40 aggregation with early intermediates already formed within the next 100 ms.

Morphologies of Zinc-Induced Aβ Aggregates. Figure 2 compares the morphological development of Aβ 1−40 in the presence and absence of Zn on a time scale of several minutes to several days. During the first 2 h the prevailing species in both samples were globular aggregates with diameters ranging from 5 to 25 nm. Additionally, we observed larger aggregates of irregular shapes typically ranging from 70 to 200 nm in length. Their characteristic globular domain texture indicates that they were formed by association of the smaller globular aggregates. The size of these oligomers increased with aging time, however, Zn-containing aggregates were significantly larger and denser than Zn-deficient ones. Most strikingly, while mature amyloid fibrils appeared in Zn deficient samples as early as 12 h after sample preparation (Figure 2, 12 h) they were not detected in Zn-containing samples even after 10 days. Thus, in this set of experimental conditions, particularly 2:1 Zn:Aβ molar ratios, Zn acts as an inhibitor of fibril formation.

Broad and Complex Size Distribution of Zn-Induced Aβ 1−40 Aggregates. To further analyze the composition of the aggregates observed by TEM as well as their soluble precursors, we used analytical ultracentrifugation (AUC) to investigate the oligomer size distribution of Aβ directly in solution by sedimentation velocity measurements (Figure 3). In these experiments, sedimenting species are resolved by the different propagation speeds of their sedimentation front monitored directly by observing radial changes in UV absorption across the sample cell; the larger the species, the faster the sedimentation speed. Very large particles (typically in the order of 10^5 kD) completely sediment during the initial centrifugation period (about 5 min) thereby preceding the first optical reading and cannot be detected.

Fresh solutions of Zn-free samples showed a single peak corresponding to low molecular weight species of Aβ 1−40 (Figure 3a,b). The peak maximum corresponded to the molecular weight of 4000 D, indicating that Aβ 1−40 was primarily monomeric. However, the peak was broader than the one observed in 10 mM NaOH (not shown) which implies the presence of small oligomers similar to the prefibrillar aggregates previously detected by photoinduced cross-linking of unmodified proteins (PICUP) analysis.[28] However, we could not resolve any specific oligomers presumably due to the sensitivity limitation of the detection system. In 3-days-old samples, the total

(28) Bitan, G.; Lomakin, A.; Teplow, D. B. *J. Biol. Chem.* **2001**, *276*, 35176−35184.

absorbance was only 35% of that observed in fresh samples, indicating that most of the peptide formed aggregates that are too large to be detected. The remaining species in solution featured discrete size distribution comprised of 82.8% Aβ 1−40 monomers, and other aggregates with oligomer numbers of approximately 20, 50, 150, 300, 500, and 1000 (Figure 3c). In freshly prepared samples containing Zn:Aβ molar ratios of 1:10, 1:2, and 1:1, the total absorbance was immediately reduced to 72%, 57%, and 15%, respectively, of that observed in fresh Zn-free samples (Figure 3a) indicating the rapid and Zn-dependent Aβ aggregation. Notably, already at 1:1 molar ratio, the total absorbance was at the instrument detection limit. Therefore, higher molar ratios were not tested. The remaining species in solution featured a much broader size distribution with respect to the Zn-free samples. Thus, a consequence of Zn-Aβ 1−40 interactions, which accelerates Aβ 1−40 aggregation rates and inhibits fibril growth, is the formation of a aggregates with a wide range of molecular weights rather than a few discrete ones in the case of slower aggregation process without Zn.

Zn-Invariant Core Structure of Aβ Supramolecular Assemblies. Using grazing incidence X-ray diffraction (GIXD), it was demonstrated that Aβ peptides readily organize at air−water interfaces because of their amphipathic nature.[29,30] Here, we show that GIXD patterns from Aβ 1−40 samples indicate similar two-dimensional lateral ordering in the presence and absence of Zn (Figure 4a). The molecular organization of both samples gives rise to two Bragg peaks with typical *d*-spacing, labeled $d_{(10)}$ and $d_{(01)}$, of 4.76 Å, and 39 Å, respectively. The thickness L_z of the crystalline film is 14 ± 5 Å, and the lateral coherence lengths, $L_{xy(10)}$ and $L_{xy(01)}$, are 100 Å and 200 Å, along the $a^*(10)$ and b^* (01) directions respectively, which corresponds to ∼20 molecules organized along the *a*-axis and ∼5 molecules organized along *b*-axis. These results are very similar to those obtained by Ege et al.[29] for Aβ 1−40 at the water surface. Furthermore, by comparison to X-ray fiber diffraction[31] and solid-state NMR[26] data obtained for Aβ 1−40 fibrils, it is possible to assign the resulting *d*-spacings to the typical dimensions of Aβ 1−40 β-hairpins in a cross-β sheet conformation. Thus, $d_{(10)}$ of 4.76 Å corresponds to the intermolecular N−H···O distances, whereas $d_{(01)}$ of 39 Å and L_z of ∼14 Å correspond to the lateral cross section of the β-hairpin in a plain perpendicular to the fibril axis (Figure 4b). These structural parameters suggest that Aβ 1−40 assembles in strands of amphipathic β-hairpin monomers with the long strand axis parallel to the air-buffer interface, the hydrophobic C-terminal segments of the hairpin facing the air, and the hydrophilic hairpin side and disordered N-terminal part facing the buffer. Structural models based on solid-state NMR indicate that such strands are actually the structural precursors of Aβ 1−40 protofibrils and fibrils. Hydrophobic interactions drive the assembly of two or more strands into fibrils with a hydrophobic core.[26,32]

Four Distinct Zn-Peptide Environments Identified by Time-Resolved X-ray Absorption Spectroscopy. To further explore the types and structures of local Zn-Aβ 1−40 environments that evolve during early stages of the aggregation reaction we have used stopped-flow freeze-quench X-ray absorption spectroscopy (XAS) procedures.[24] XAS spectral analysis provides local structural information about the nearest coordination environment surrounding the metal ion absorber within the protein moiety in solution. Combining XAS with kinetic stopped-flow methods provides insights into the lifetimes and local atomic structures of metal-protein intermediates in millisecond to minute time scales.[24] Here, we used this method to correlate the observed kinetic phases (Figure 1) with the local structure of transient Zn-Aβ 1−40 intermediates that evolve during the initial interaction of Zn with Aβ 1−40 under the reaction conditions. The freeze-quench apparatus has a shorter

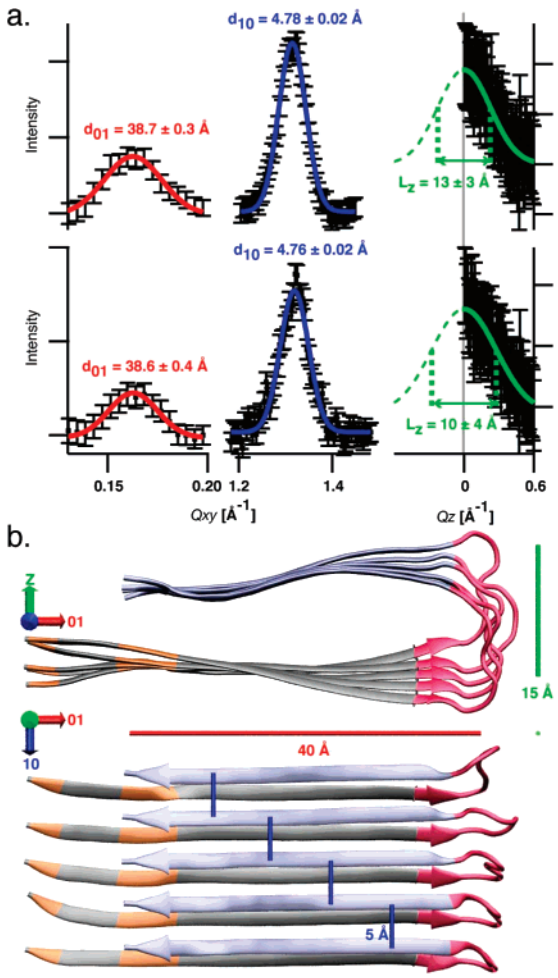

Figure 4. Cross β-hairpin structure of Aβ 1−40 with and without zinc. a. GIXD spectra of Zn-free (top) and Zn-containing (bottom) Aβ 1−40 films at air-buffer interfaces. Lateral ordering gives rise to very similar Bragg peaks in the Q_{xy} plane, parallel to the air−buffer interface. These were fit with Gaussian curves to yield two *d*-spacing values, d_{01} and d_{10} (red and blue, respectively). The full width at half-maximum of the Bragg rods along the perpendicular Q_z direction (green) yielded the crystalline film thickness, L_z. b. The typical dimensions of Aβ 1−40 $d_{01} \approx 5$ Å, $d_{10} \approx 40$ Å, and $L_z \approx 15$ Å (red, blue, and green bars, respectively) are in very good agreement with a recent solid-state NMR structural model of Aβ 1−40 fibrils.[22] It suggests that Aβ 1−40 monomers acquire an amphipathic β-hairpin conformation in a plane perpendicular to the air−water interface with the hydrophobic and hydrophilic β-strands (light blue and gray, respectively) facing the air and buffer sides, respectively. Hydrogen-bonding drives the stacking of β-hairpins along the air−water interface thereby forming a single amphipathic fibrillar strand. The hairpin bend region, residues 22−29, is pink, and residues Y10, H13, and H14 are orange.

(29) Ege, C.; Majewski, J.; Wu, G. H.; Kjaer, K.; Lee, K. Y. C. *ChemPhysChem* **2005**, *6*, 226−229.
(30) Maltseva, E.; Kerth, A.; Blume, A.; Mohwald, H.; Brezesinski, G. *ChemBioChem* **2005**, *6*, 1817−1824.
(31) Malinchik, S. B.; Inouye, H.; Szumowski, K. E.; Kirschner, D. A. *Biophys. J.* **1998**, *74*, 537−545.
(32) Petkova, A. T.; Ishii, Y.; Balbach, J. J.; Antzutkin, O. N.; Leapman, R. D.; Delaglio, F.; Tycko, R. *Proc. Natl. Acad. Sci. U.S.A.* **2002**, *99*, 16742−16747.

dead time than the stopped-flow setup, therefore, we rapidly mixed and froze ten samples within a range of 2−2000 milliseconds after mixing Aβ 1−40 with 2 molar equivalents of Zn according to the observed transient kinetic traces for this reaction condition (Figure 1).

Figure 5 a represents the raw X-ray absorption near edge data (XANES) (left panel) and the background subtracted X-ray absorption fine structure (EXAFS) data (right panel). To determine the number of distinct Zn-binding conformers and to identify the most representative XAS spectra for each site, we used principal factor analysis (PFA)[25] which indicated four distinct Zn-protein environments (Figure 5b). Since deconvolution of XAS data sets into their underlying pure spectral components is not yet feasible for mixtures of more than two components in dilute protein solutions,[33] we used iterative key set factor analysis (IKSFA) to select a set of four characteristic spectra (Figure 5c) and four key time points that best represent the spectral variation in the complete data set. These are presented in the form of Fourier transform (FT) spectra to provide the radial distribution of the various protein residue atoms within the first and second coordination shells around the Zn center. The shape and amplitude of the first FT peaks are directly related to the type and number of the amino acid residues/ligands that are bound to the Zn ion. Thus, the spectral changes observed among the different time domains indicate variations of the local protein environment around the Zn ion. These variations can be due to the presence of different Zn binding sites and/or structural transformations around the Zn ion within its protein complex. Altogether, our results strongly suggest that multiple Zn binding sites are present within Aβ 1−40 aggregates.

Discussion

The recently observed local and rapid discharge of extracellular Zn from Zn-releasing neurons during normal brain function has prompted us to study the kinetics of Zn binding and misfolding of Aβ on a similar time-scale. Using rapid mixing techniques in a stopped flow apparatus we simulated typical synaptic Zn release conditions and directly observed rapid changes in Aβ 1−40 conformation and aggregation states, on the order of milliseconds, by recording Y10 fluorescence, and Rayleigh light scattering intensity, respectively. The long-term consequences of these rapid Zn-Aβ interactions were revealed by TEM and AUC. The first provided direct information on the actual morphology of Aβ 1−40 at various stages of aggregation with a spatial resolution of ∼2−3 nm, and the latter revealed the actual size distribution of Aβ 1−40 in solution. The results from both methods indicate that stoichiometric quantities of Zn dramatically alter Aβ 1−40 aggregation pathways in solution. Without Zn, fibrils are formed in a slow process over several hours to few days and the aggregate size distribution comprises only several distinct oligomer sizes. Adding Zn to Aβ 1−40 results in immediate formation of a broad distribution of aggregates, but no fibrils eventually form. Most importantly, our TEM results have shown that Zn inhibits the formation of Aβ 1−40 fibrils and stabilizes non-fibrillar forms with small spherical morphologies that resemble the more pathogenic aggregation intermediates of Aβ 1−40[11,34−37]

Our kinetic, TEM, and AUC results demonstrate that stabilization of non-fibrillar aggregates and inhibition of fibrillar forms of Aβ 1−40 are rapidly triggered by interaction with Zn at micromolar concentrations. Therefore, even short transient bursts of Zn such as those occurring during synaptic release should suffice for inducing pathogenic effects via the formation of pathogenic Aβ aggregates.

To further explore the molecular details of Zn-Aβ 1−40 interactions we have capitalized on the possibility of assembling Aβ 1−40 monomers at the air−buffer interface into conformation that resemble precursors of amyloid fibrils. By using GIXD, we were able to obtain structural information from these precursors at near-molecular resolution. The invariance of Aβ 1−40 cross-β strand structures to the presence of Zn rules out Zn-Aβ 1−40 interactions that either induce major conformational changes in the amyloid fold or affect the stacking space of the ordered cross-β core structure. Thus, Zn may interact with three possible Aβ 1−40 domains: (i) the C-terminal β-strand, residues 30−40 (Figure 4b, light-blue segment), which forms the fibril core; interactions with Zn ions in this domain are unlikely because of its hydrophobic nature; (ii) the bend region, residues 23−29, including a salt bridge between residues D23 and K28 (Figure 4b, pink segment); and (iii) the N-terminal disordered region and β-strand, residues 1−8 (not shown) and 9−22 (Figure 4b, gray segment), respectively; this region comprises many putative ligands including residues Y10, H13, and H14 (Figure 4b, orange segments) that have been identified as the binding site for other metal ions such as Cu.[38−40] Importantly, the observed heterogeneity in size distribution (Figure 3) in the presence of Zn may be the consequence of the formation of multiple metal-protein sites residing in different atomic environments.

The molecular mechanisms of Zn-induced Aβ 1−40 aggregation in solution were probed by stopped-flow freeze−quench XAS procedures.[24] The rapid formation of multiple Zn-Aβ 1−40 complexes without effecting the peptide core structure, the observed heterogeneity in size distribution, and the persistence of Zn-Aβ 1−40 non-fibrillar aggregates provide novel insights into the assembly mechanism.

Recently, the formation of amyloid fibrils was shown to occur via intersheet alignment process.[41] In this mechanism, the β-sheets realign by repeated detachment and annealing of strands in solution and local realignment of polypeptide strands within an aggregate.[41] In light of this, rapid binding of zinc ions to

(33) Frenkel, A. I.; Kleifeld, O.; Wasserman, S. R.; Sagi, I. *J. Chem. Phys.* **2002**, *116*, 9449−9456.
(34) Dahlgren, K. N.; Manelli, A. M.; Stine, W. B.; Baker, L. K.; Krafft, G. A.; LaDu, M. J. *J. Biol. Chem.* **2002**, *277*, 32046−32053.
(35) Chromy, B. A.; Nowak, R. J.; Lambert, M. P.; Viola, K. L.; Chang, L.; Velasco, P. T.; Jones, B. W.; Fernandez, S. J.; Lacor, P. N.; Horowitz, P.; Finch, C. E.; Krafft, G. A.; Klein, W. L. *Biochemistry* **2003**, *42*, 12749−12760.
(36) Hoshi, M.; Sato, M.; Matsumoto, S.; Noguchi, A.; Yasutake, K.; Yoshida, N.; Sato, K. *Proc. Natl. Acad. Sci. U.S.A.* **2003**, *100*, 6370−6375.
(37) Lambert, M. P.; Barlow, A. K.; Chromy, B. A.; Edwards, C.; Freed, R.; Liosatos, M.; Morgan, T. E.; Rozovsky, I.; Trommer, B.; Viola, K. L.; Wals, P.; Zhang, C.; Finch, C. E.; Krafft, G. A.; Klein, W. L. *Proc. Natl. Acad. Sci. U.S.A.* **1998**, *95*, 6448−6453.
(38) Atwood, C. S.; Moir, R. D.; Huang, X. D.; Scarpa, R. C.; Bacarra, N. M. E.; Romano, D. M.; Hartshorn, M. K.; Tanzi, R. E.; Bush, A. I. *J. Biol. Chem.* **1998**, *273*, 12817−12826.
(39) Atwood, C. S.; Perry, G.; Zeng, H.; Kato, Y.; Jones, W. D.; Ling, K. Q.; Huang, X. D.; Moir, R. D.; Wang, D. D.; Sayre, L. M.; Smith, M. A.; Chen, S. G.; Bush, A. I. *Biochemistry* **2004**, *43*, 560−568.
(40) Schoneich, C.; Williams, T. D. *Chem. Res. Toxicol.* **2002**, *15*, 717−722.
(41) Petty, S. A.; Decatur, S. M. *Proc. Natl. Acad. Sci. U.S.A.* **2005**, *102*, 14272−14277.

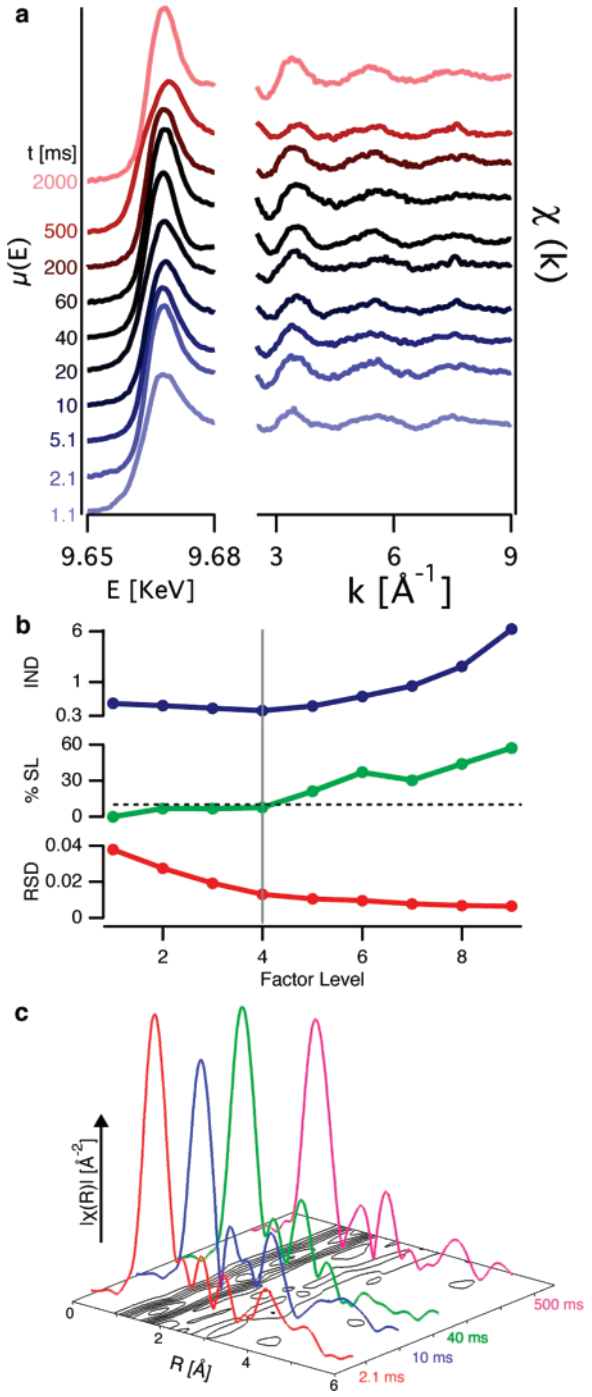

Figure 5. (a) X-ray absorption near edge (left) and background subtracted X-ray absorption fine structure (right) spectra (XANES, and EXAFS respectively) of Zn-Aβ 1−40 samples collected along the kinetic trace presented in Figure 1. Numbers to the left of each spectrum indicate the aging times in ms of each sample. (b) The complete set of spectra was subject to factor analysis and the data was examined by three criteria: residual standard deviation (RSD, red trace), Malinowski F-test converted into percent significance level (%SL, green trace), and Malinowski indicator function (IND, blue trace) as a function of factor level. All three criteria consistently indicate the presence of four independent spectral components above the noise level. The factor level at which RSD levels off, %SL indicates 90% degree of confidence (dashed line) and IND reaches a minimum at a factor level of four. (c) IKSFA was used to select the four key spectra that best represent the complete data set. These were found to be at 2.1, 10, 40, and 500 ms, and their FT-EXAFS are shown in red, blue, green, and magenta, respectively, over a contour plot representing the complete set of FT-EXAFS spectra. Spectral variation at the first and the second coordination shells are clearly observed above the noise level indicating local structural differences at nearest Zn environments.

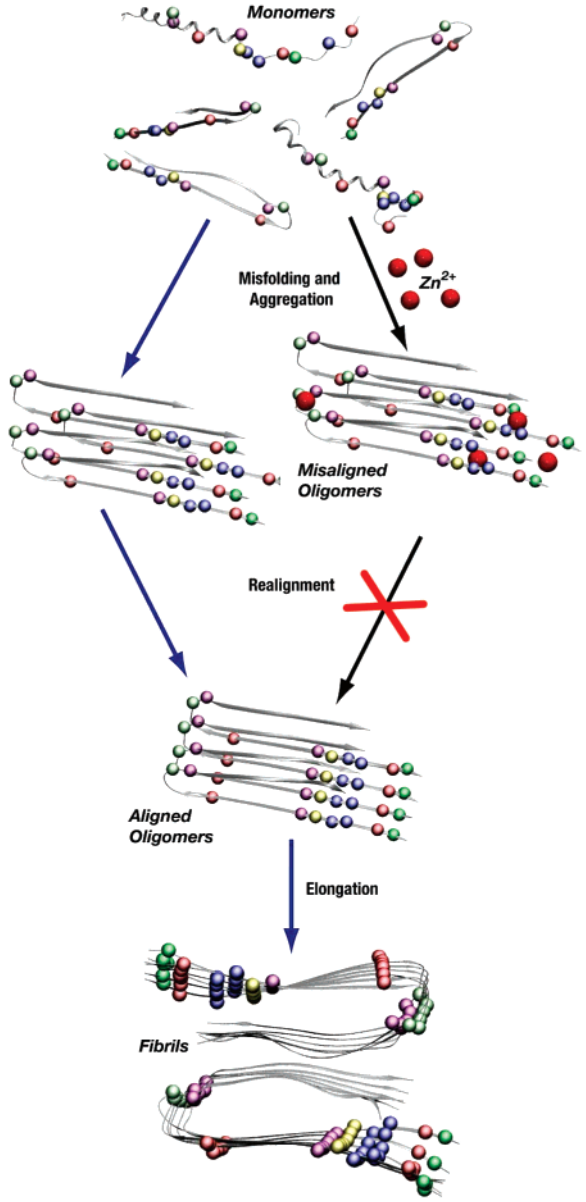

Figure 6. Proposed mechanism of the role of Zn in Aβ aggregation process. In the absence of perturbation, fibrils are formed by misfolding and aggregation of Aβ monomers followed by the intersheet alignment mechanism (blue arrows). The rapid binding of Zn ions (red spheres) to multiple sites within Aβ aggregates interferes with this process (black arrows). Possible binding sites are marked by light green, yellow, red, blue, green, and purple beads representing asparagine, glutamine, glutamate, histidine, tyrosine, and lysine, respectively, which are putative ligands of Zn ions. The rapid interchelation of Zn ions to this complicated network of multiple intra- and intermolecular Zn-binding sites prevents realignment and formation of fibrillar aggregates.

multiple Aβ 1−40 sites (reported here) may interfere with realignment by practically locking the relative positions of the β-sheet peptide cores (Figure 6), thus preventing realignment and inhibiting fibril growth. Consequently, the lifetimes of pathogenically related non-fibrillar intermediates are prolonged.

The concept of zinc perturbing intersheet alignment may be generalized to other fibril growth inhibitors. Remarkably, perturbation of Aβ fibril growth and stabilization of smaller and more neurotoxic aggregates has been reported to occur by chemical[34,35] or mechanical[36] treatment as well as by specific

proteins such as clusterin (apolipoprotein J).[37] Bitan et al.[42] have identified similar globular particles as precursors of protofibrils, another neurotoxic oligomeric form of Aβ that precedes fibril formation. Thus, in this general context, the pathogenic effects of Zn are probably the consequence of stabilizing toxic Aβ forms and preventing formation of the more benign amyloid fibrils.

The proposed mechanism provides a novel view on the pathological role of Zn ions in developing of Alzheimer's disease bridging binding effects in the millisecond time domain with accumulation of pathogenic aggregates over years.

Conclusions

By using time-resolved structural and spectroscopic techniques, we have shown, for the first time, that interactions between Zn and Aβ 1−40 occur in less than a millisecond and initiate Aβ 1−40 conformational changes and aggregation in a few milliseconds. On a longer time-scale, TEM and AUC indicate that these interactions prevent the formation of the typical amyloid fibrils, and induce the accumulation of large unorganized aggregates of smaller non-fibrillar forms of Aβ, which have been previously implicated as pathogenically related forms of AD.

Here, we propose a general pathogenic pathway, in which Zn represents a class of molecular pathogens that effectively stabilize transient, toxic pre-aggregate amyloid forms by interfering with the process of Aβ self-assembly which leads to insoluble, non-pathological fibrillar forms. The new molecular insights presented here underline the importance of rapid kinetics in stabilizing pathogenic Aβ aggregate and demonstrate the viability of structural dynamic studies for understanding the pathological processes of AD and other amyloid-related disorders, and their potential for drug discovery.

Acknowledgment. We thank Dr. Gal Bitan of the Department of Neurology, David Geffen School of Medicine, UCLA, Los Angeles, CA and Dr. Jonathan Friedman, D-Pharm Ltd., Rehovot, Israel, for critical reading of the manuscript and useful discussions, Dr. Robert Tycko, Laboratory of Chemical Physics, NIDDK, National Institutes of Health, Bethesda MD, for providing us with the coordinates of his NMR-based Aβ 1-40 structural model, and Sara Rubinrat, Organic Chemistry Department, Weizmann Institute of Science, Rehovot, Israel, for the synthesis of Aβ peptides. We acknowledge financial support from the estate of David Turner. We thank the HASYLAB at Hamburg and the Kimmelman center at the Weizmann Institute for providing synchrotron beam time and traveling support respectively. D.N. acknowledges a long-term fellowship from the Human Frontiers Science Program Organization. K.K. acknowledges support by the Carlsberg Foundation and the DanSync program of the Danish Natural Science Research Council. I.S. is incumbent of the Clotide and Mauricio Pontecorvo Professorial Chair.

Supporting Information Available: Scheme of mixing sequence for proper normalization of signal intensities from Zn/Aβ 1−40 mixtures. This material is available free of charge via the Internet at http://pubs.acs.org.

JA076282L

(42) Bitan, G.; Kirkitadze, M. D.; Lomakin, A.; Vollers, S. S.; Benedek, G. B.; Teplow, D. B. *Proc. Natl. Acad. Sci. U.S.A.* **2003**, *100*, 330−335.